Experimental Investigation of Plasma Production by Irradiating Solid Hydrogen Foils with an Intense Pulse Laser

R. SIGEL *

Institut für Plasmaphysik, Garching bei München

(Z. Naturforsch. **25 a**, 488—503 [1970]; received 22 December 1969)

Foils of solid hydrogen were irradiated with a giant pulse ruby laser. The formation and expansion of the plasma produced this way was investigated by time-resolved absorption measurements, by streak and framing photography, by holographic interferometry and by time-off-flight and charge collection measurements. The measurements yield a fairly complete picture of this process: After the initial breakdown in the solid a plasma is produced at the surface of the foil facing the laser. Owing to the high pressure of the plasma the solid hydrogen is compressed by a shock wave. This allows the layer in which the plasma is produced to penetrate into the interior of the foil with a velocity of 3×10^6 cm/sec. Thus under the action of the focused beam foils up to 1 mm thickness are pierced by the light before the end of the pulse. The plasma cloud, ejected towards the laser, contains 4×10^{16} ions with a mean kinetic energy of 200 eV this corresponding to about half of the absorbed energy. The observations are compared with the well known results obtained in a plane, one-dimensional geometry. If allowance is made for the influence of the focusing of the laser beam on the structure of the shock front, the observations are readily understood.

I. Introduction

Giant pulse lasers that emit a single, extremely intense light pulse lasting a few nanoseconds have been available for a few years now. By focusing the laser beam a hot plasma can be poduced on the surface of a solid by the incident light.

Hydrogen and deuterium plasmas produced by irradiating these materials in the solid state are meeting with increasing interest in fusion research. In most of the experiments performed until now [1–4] the aim has been to produce an isotropically expanding plasma by completely evaporating a small speck of the material. A plasma cloud produced in this way would be useful for heating and confinement experiments because of its unique properties.

The experiment described here was not intended with any specific application in mind, but was conducted to create the best possible conditions for investigating the process of plasma production by intense laser light on the surface of solid hydrogen. Apart from the fact that this interaction process in itself is of interest, understanding of it might be helpful in planning applications of plasmas produced this way. For example, it may be useful for interpretating the experiments with small specks of solid hydrogen mentioned above, where no isotropic expansion of the plasma occurred except in [3].

In this experiment self-supporting solid hydrogen foils in high vacuum are irradiated with a ruby laser. Foils of different thicknessess are used in an effort to observe the foil surface on the opposite side from the laser instead of observing the processes occurring in the more inaccesible interior of a solid block. The intensity in the focal spot is about 10^{12} W/cm^2, which is typical of the intensities that can readily be attained at present.

The process of plasma formation by intense laser radiation has been investigated theoretically by various authors [5–7] in one-dimensional, plane geo-

* Auszug aus der von der Fakultät für Maschinenwesen und Elektrotechnik der Technischen Hochschule München genehmigten Dissertation „Experimentelle Untersuchung der Plasmaerzeugung durch fokussierte Laserstrahlung an Folien aus festem Wasserstoff" des Dipl.-Phys. RICHARD SIGEL. Tag der Promotion 6. August 1969.
Sonderdruckanforderungen an Dr. S. WITKOWSKI, Institut für Plasmaphysik GmbH, Experimentelle Plasmaphysik 3, *D-8046 Garching* bei München.

[1] U. ASCOLI-BARTOLI, E. MAZZUCATO, and C. DE MICHELIS, Conf. Plasma Physics and Controlled Nuclear Fusion Research Culham **2**, 941 [1965].
[2] P. A. H. SAUNDERS, P. AVIVI, and W. MILLAR, Phys. Lett. **24 A**, 290 [1967].
[3] G. FRANCIS, D. W. ATKINSON, P. AVIVI, J. E. BRADLEY, C. D. KING, W. MILLAR, P. A. H. SAUNDERS, and A. F. TAYLOR, Phys. Lett. **25 A**, 486 [1967].
[4] U. ASCOLI-BARTOLI, B. BRUNELLI, A. CARUSO, A. DE ANGELIS, G. GATTI, R. GRATTON, F. PARLANGE, and A. SALZMANN, Plasma Physics and Controlled Nuclear Fusion Research (Vienna: International Atomic Energy Agency), Paper CN-24/F-6 [1969].
[5] YU. V. AFANASYEV, O. N. KROKHIN, and G. V. SKLIZKOV, IEEE J. Quantum Electronics **2**, 483 [1966].
[6] A. CARUSO and R. GRATTON, Plasma Phys. **10**, 867 [1968].
[7] P. MULSER, Dissertation TH München [1969] and Laboratory Report IPP 3/95; Z. Naturforsch. **25 a**, 282 [1970].

metry. Apart from achieving the focusing necessary for high intensity, the use of plane foils comes closest to this geometry. The experiment is therefore expected to yield information on the validity of these theoretical studies.

II. Experimental Set-Up

The experimental set-up is sketched in Fig. 1. It is composed essentially of the *laser*, the *cryogenic system* for producing solid hydrogen foils, and the *vacuum chamber*.

The *laser* is a twostage ruby laser (model Korad K-1500). It emits a single giant pulse with an energy $E_L = 2.9$ joule (with allowanve for reflection losses up to the target) lasting $\tau = 18$ nsec (half-width). From the measured angular divergence of the laser ($\Theta = 1.4 \times 10^{-3}$ rad for half the energy) it is calculated with $\Theta = 2\,r/f$ for the lens (focal distance $f = 5$ cm) used here that half the energy is focused on a circular area $2\,r = 0.07$ mm in diameter. With respect to the aberrations of the uncorrected, planoconvex lens, it is assumed somewhat arbitrarily that the total energy is distributed over a circular area with the diameter $2\,r_0 = 0.14$ mm. With this value the calculated intensity in the focal spot is

$$\Phi = E_L(\pi\, r_0^2\, \tau)^{-1} = 1 \times 10^{12}\ \mathrm{W\,cm^{-2}}.$$

The horizontally polarized beam emerges from the amplifier ruby (Brewster end, diameter 3/4″) obliquely to the laser axis and passes through the base into an equilateral 90° glass prism (10 in Fig. 1) almost without reflection loss (angle of incidence ≈ Brewster angle). On emerging the beam again becomes parallel to the axis of the laser. Furthermore, the cross section of the beam, which is elliptical between the amplifier ruby and the prism, again becomes almost circular. About 4% of the light is reflected at the exit surface of the prism and emerges at an angle of 90° to the main beam after being totally reflected at the base of the prism. This part of the beam is used for measuring the energy of the laser pulse at every shot. In the energy meter (11) the light is scattered onto a semiconductor photodiode (hp 2−4220, rise time < 1 nsec) the signal of which is integrated by means of a RC-network.

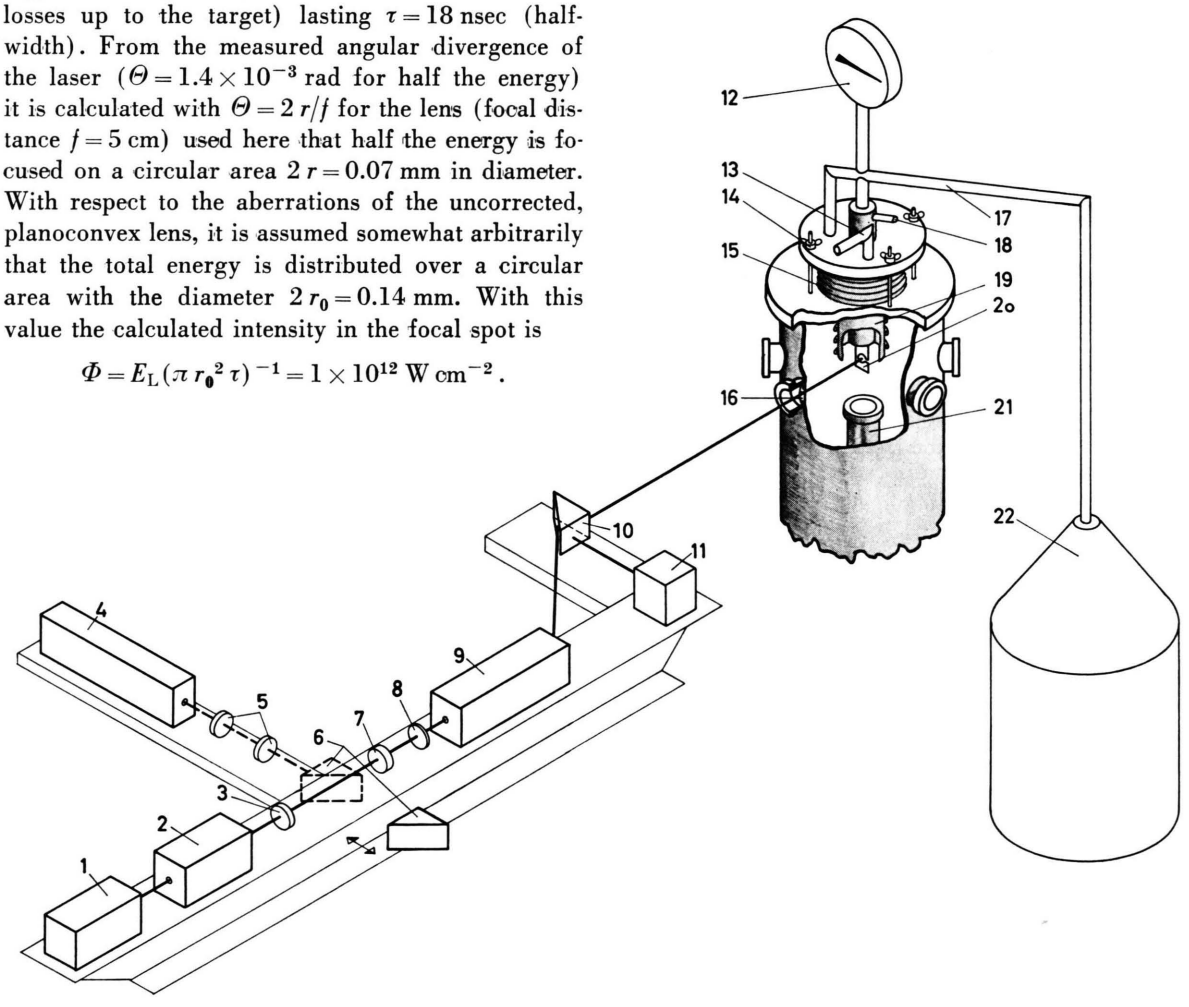

Fig. 1. Experimental set-up. 1. Pockels cell. 2. Oscillator. 3. Mirror. 4. Adjustment laser (He-Ne gas laser). 5. Telescope. 6. Prism for reflecting the adjustment laser. 7.—8. Telescope. 9. Amplifier. 10. Prism. 11. Energy meter. 12. Gauge (vapour pressure thermometer). 13. Helium exhaust. 14. Adjusting screws. 15. Bellows. 16. Focusing lens. 17. Helium transfer line. 18. Hydrogen inlet. 19. Cu jacket. 20. Cooling finger. 21. Bell glass. 22. Helium container.

The instrument was calibrated with the liquid calorimeter described in [8]. The ruby laser beam can be simulated by an adjustment laser (4) (He-Ne gas laser). The beam of this laser is adjusted after expansion (5) into the axis of the ruby laser by a totally reflecting prism (6) that is pushed aside prior to each laser shot. The Pockels cell (1) used as Q-switch in the oscillator stage allows the ruby laser to be synchronized with the electronic measuring instruments (oscilloscope, image converter camera) by a common electric trigger pulse.

The *cryogenic system* for producing the self-supporting solid hydrogen foils is described in detail in [9]. We therefore only briefly review how it works:

A cooling finger (20) (1 mm thick copper sheet) is cooled in a hydrogen atmosphere by liquid helium from a supply container (22). Liquid hydrogen condensing on the cooling finger then runs down and covers the hole in the finger by virtue of its surface tension. This forms an initially liquid film which can be frozen without striation by further cooling. When the bell glass (21) separating the space around the cooling finger from the high vacuum during these processes is withdrawn from below, a self-supporting disc of solid hydrogen is left in the hole of the cooling finger. The finger (20) is shown with such a disc in Fig. 2. The discs are fairly clear and transparent (solid hydrogen being a colourless crystal). The diameter is 2 mm, in keeping with the diameter of the hole. Immediately after the bell glass is withdrawn the thickness is approximately $1-1.5$ mm. This slowly decreases owing to the sublimation at the surface of the foil; after about 15 min the disc disappears. As the thickness of these discs therefore becomes small relative to the diameter, they are usually denoted in the following as foils. In the experiment the laser is fired when the disc attains the required thickness.

As the hole in the cooling finger is slit, both surfaces of the foil can be observed from the side. The thickness of the foil is measured with a long-focus microscope. While the foil slowly sublimates, the pressure in the container is about 1×10^{-5} Torr.

The cylindrical *vacuum chamber* (20 cm in diameter) is evacuated by a diffusion pump. On a level with the beam it has eight observation windows all the way round, one of which is occupied by the focusing lens (16). The remaining windows can be replaced ad hoc by vacuum tight lens mounts, leadthroughs for probes, etc.

The cooling finger was adjusted by means of an intervening bellows (15) of large diameter. In addition, the focusing lens could be shifted in the beam direction. The adjustmen laser was used to center the focal spot of the pulse laser on the hydrogen disc. The plane of narrowest cross section was adjusted in the midplane of the foil with an accuracy of about ± 0.3 mm. No critical focusing dependence of any of the measured values was observed. The pulse laser, adjustment laser, and vacuum chamber are mounted on a stable metal table (not shown in Fig. 1).

III. Experimental Investigations

1. Absorption and Reflection Measurements

In this experiment a plane transparent foil is placed in the focal spot. The time-dependent absorption behaviour of the foil can therefore be determined by comparing the pulse shape of the incident and transmitted light. The light reflected from the target (at least part of it) leaves the vacuum vessel through the focusing lens. Its time behaviour can therefore be measured as well and compared with that of the incident laser light.

The measuring set-up is composed of three photodiodes D1 – D3 for determining the time behaviour of the laser light incident on the target (D1), transmitted by it (D2), and reflected from it (D3). They are arranged as in Fig. 3. The photodiodes are interconnected by long coaxial cables acting as delay lines. At each

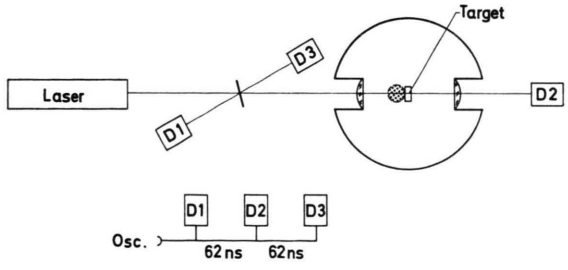

Fig. 3. Arrangement of photodiodes for measuring the absorption and reflection behaviour of the foil. Below: circuitry of the photodiodes.

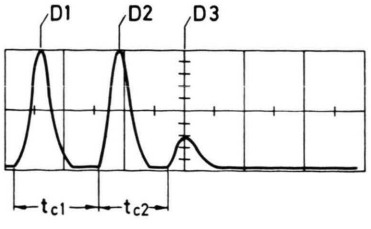

Fig. 4. Signals of the photodiodes D1 – D3 without foil. D1 incident laser light, D2 transmitted laser light, D3 reflected laser light. 50 nsec/div.

[8] R. SIGEL, Laboratory Report IPP 3/86 [1969].

[9] R. SIGEL, H. KRAUSE, and S. WITKOWSKI, J. Sci. Instrum. Ser. 2, **2**, 187 [1969].

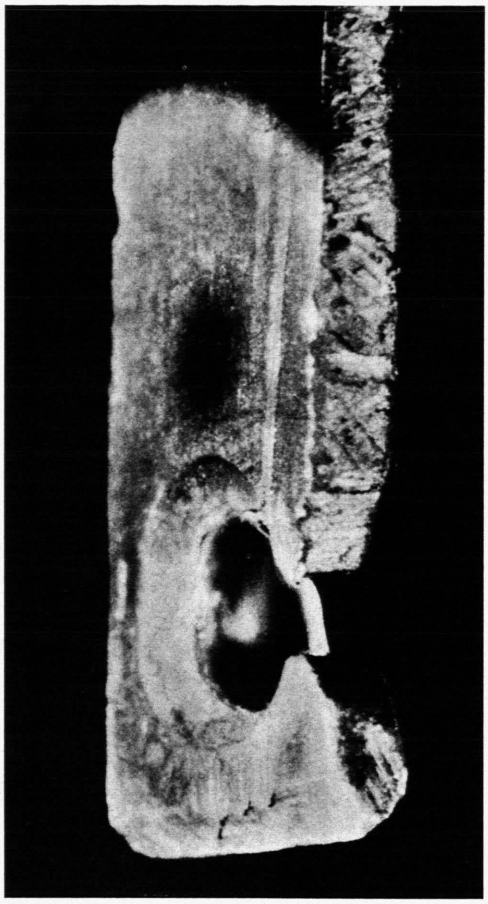

Fig. 2.

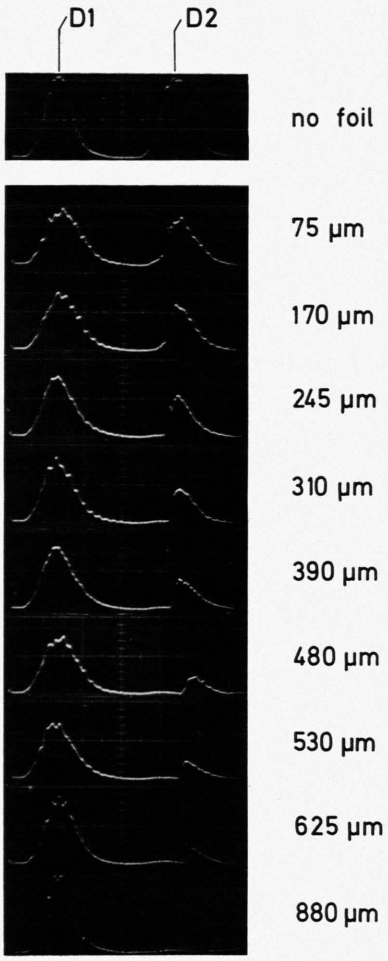

Fig. 5.

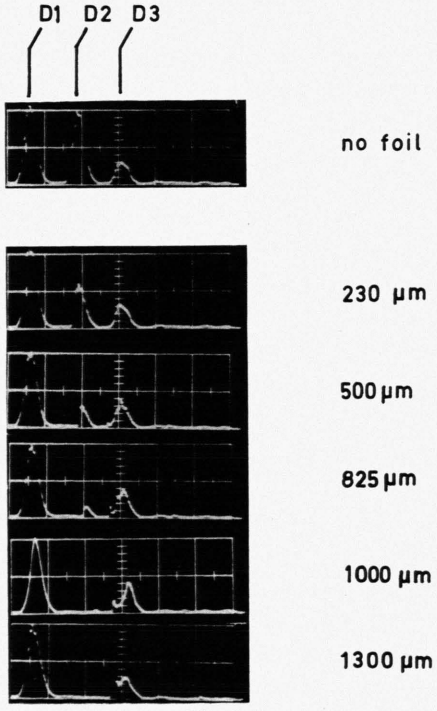

Fig. 8.

Fig. 2. Cooling finger with solid hydrogen disc. Diameter of the hole 2 mm. The adjustment laser is focused into the center of the disc.

Fig. 5. Oscillograms with the signals of the photodiodes D1 and D2 for foils of various thicknesses. 20 nsec/div.

Fig. 8. Oscillograms with the signals of the photodiodes D1 to D3 for foils of various thicknesses. 50 nsec/div.

laser shot the pulses of the three photodiodes appear successively on the oscilloscope screen without overlapping (Fig. 4). The order of the pulses corresponds to the circuitry of the diodes (Fig. 3, bottom).

The diodes D1 and D2 were balanced by means of filters (including a filter for suppressing the light emission of the plasma) so that the signals of the two diodes are equal when no foil is present. The filters in front of D3 are less dense so that without a foil the photodiode D3 also emits a pulse that is caused by stray light. The pulses follow at intervals t_{c1} and t_{c2} governed mainly by the length of the cables (corresponding to 62 nsec in each case). These intervals slightly differ within a few nanoseconds because of the different transit times of the light from the laser to the individual photodiodes. The photodiodes are vacuum photodiodes ITT F 4000 (S1 cathde) with a rated rise time of 0.3 nsec. The oscilloscope is a Tektronix 519 with a rise time of likewise 0.3 nsec and a vertical sensitivity of 10 V/cm. It was triggered internally. In order to prevent the rise of the signal of the photodiode D1 from being more or less curtailed, depending on the choice of trigger voltage, the signals were delayed 20 nsec by inserting a cable in the oscilloscope between the pick-up point of the trigger signal and the image tube. The beam then has to cover a short distance on the screen before the signal reaches the image tube and vertical deflection sets in.

Absorption measurements: Fig. 5 shows a set of oscillograms of the signals of only the photodiodes D1 and D2 for foils of different thicknesses. As can be seen, the intensity of the transmitted laser light has a definite time behaviour, especially for the thicker foils. This is illustrated in Fig. 6, where the signals of the two photodiodes are again shown. For comparison the time behaviour of the incident laser light is traced above the curve of the transmitted laser light. During a certain time, the burn-through time t_D, the foils prove to be opaque to the incident laser light. As the reflection measurements described later show, the laser light is completely absorbed during this time. This interval of strong absorption is followed by a discontinuous rise in the intensity of the transmitted laser light. From this time the laser light can pierce the foil with comparatively low absorption. t_D is measured from the beginning of the laser pulse as observed on the oscilloscope screen. (The well defined beginning of the pulse on the screen is due to a nonlinear behaviour of the T-junctions of the cables for signals less than 0.4 V. For details see [10].) This, however. is not very arbitrary, since the beginning of self-luminosity, indicating strong heating of the foil, coincides with this moment within a few nanoseconds (see streak photograph Fig. 11). Within this limit breakdown may also shift somewath, depending on the focusing of the beam. This fact is considered responsible for the lengthening of t_D reported in a previous paper [11] covering the first shots, for which a more simple set-up was used. As these uncertainties in the choice of the beginning of t_D are small compared with the burn-through time of thick foils ($d \approx 1$ mm), they do not affect the conclusions drawn from the measurements (see Section IV).

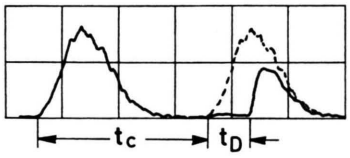

Fig. 6. Comparison between incident and transmitted laser light.

The burn-through time t_D increases with the foil thickness. Foils which are thicker than about 1 mm do not become transparent before the end of the pulse. t_D was determined as a function of the foil thickness d from 90 oscillograms. The experimental points cover a period of 30 nsec, corresponding to the length of the laser pulse. The linear relationship between t_D and d shown in Fig. 7 was found. The mean quadratic error of the experimental values, grouped according to t_D, is given.

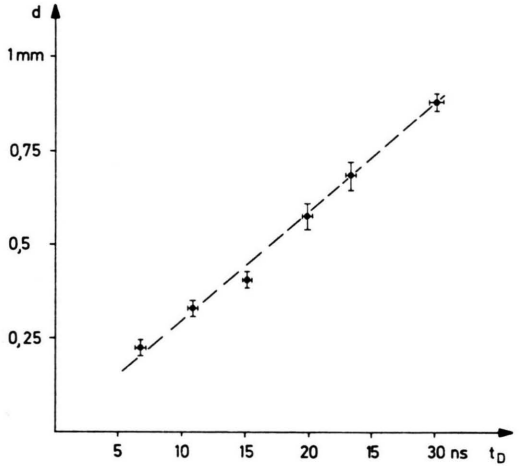

Fig. 7. Foil thickness d as a function of the burn-through time t_D.

[10] R. SIGEL, Dissertation TH München [1969] and Laboratory Report IPP 3/96 [1969].

[11] R. SIGEL, K. BUECHL, P. MULSER, and S. WITKOWSKI, Phys. Lett. **26 A**, 498 [1968].

Reflection measurements: Figure 8 shows a set of oscillograms for which the photodiode D3 was incided with the potodiodes D1 and D2 to measure the reflected laser light. For clarity the time variations of the signals are again plotted separately in Fig. 9. Comparison between the oscillograms taken with and without foil in Fig. 8 shows that the laser light reflected from the foils does not increase the amount of scattered light present, irrespective of the thickness of the foil. Since complete reflection of the laser light back through the lens would correspond to a signal of D3 10^3 times as high as that of D1, the measurements show that practically all the incident energy is absorbed or transmitted by the target. A short pulse P1 of reflected laser light occurring at the beginning of the laser pulse was, however, observed (Figs. 8, 9). Its intensity increases with the thickness of the foils. The cause of this pulse was not investigated. It may, however, be due to Fresnel reflection from the vacuum-solid interface, which is still intact at this early time. With thick foils the intensity required for breakdown is not reached at the surface of the foil till a somewhat later time (the laser always being focused in the midplane of the foil). The increases of P1 with foil thickness could then be explained by the fact that with thicker foils more light can be reflected before the surface is destroyed.

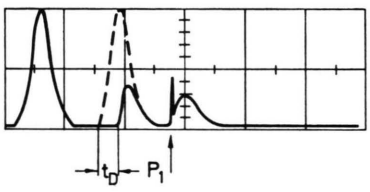

Fig. 9. Comparison between incident, transmitted, and reflected laser light.

2. *Streak Photography with an Image Converter Camera*

In order to investigate the process of plasma production on the foil by means of the light emission of the matter, streak pictures of the foil were made with an image converter camera. Observation was made perpendicularly to the laser beam, i. e. at a tangent to the surface of the foil, through the slit in the cooling finger.

The experimental set-up is shown in Fig. 10. The cooling finger with the foil is imaged by two lenses O1 and O2 on the cathode K of the image converter camera. The streak slit Sp is located in the intermediate image in front of a field lens F. It is placed parallel to the axis of the laser beam and set by means of the adjustment laser. In front of the lens O1 there is a filter GF (Schott BG 18). This prevents laser light scattered by the foil from getting into the camera and being interpreted in the pictures as light emitted by the matter.

The image converter camera (Model IPP EL 085) was operated with the maximum posible streak speed of 100 nsec/cm with respect to the camera screen. The magnification — object : intermediate image : screen — was 1 : 1 : 1. The width of the streak slit (0.1 mm)

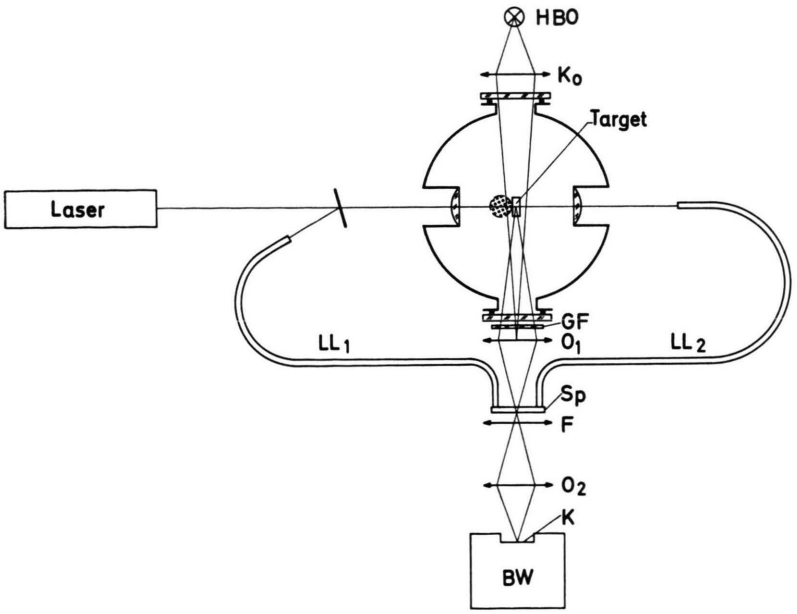

Fig. 10.
Set-up for recording streak pictures.
HBO = high-pressure mercury lamp,
Ko = condenser lens,
GF = filter,
O1 = lens,
Sp = streak slit,
LL1, LL2 = light pipes,
F = field lens,
O2 = lens,
K = cathode of image converter camera,
BW = image converter camera.

was adapted to the given resolution of the screen (10 line pairs/mm). This gives a time resolution of the order of 1 nsec. The screen was photographed with a Polaroid camera.

In order to allow the time behaviour of the light emission of the matter to be related to that of the laser, the emergence planes of two light pipes ware placed at the ends of the streak slit. The light pipes convey laser light from the front and back of the foil to the streak slit, thus producing time marks on both sides of the streak picture. With due allowance for the different transit times of the laser light and the plasma light to the streak slit, the two time marks allow the light emission of the matter to be exactly pinpointed in time relative to the time variation of the laser pulse. By comparing these time marks with the oscillograms of the photodiodes D1 – D3 taken during the same shot the time corresponding to the beginning of the laser pulse on the oscilloscope was determined and chosen as zero for the time scale.

For interpreting the phenomena involved the time at which the foil becomes transparent is of particular interest. Because of the steep rise of the transmitted laser light this time can be determined with great accuracy from the corresponding time mark. The actual instant where the foil becomes transparent to the laser light (determined with respect to the transit time of the light through the light pipe) is given by the triangle (◀) in Fig. 11. (The time mark itself is not very bright in Fig. 11 owing to the absorption of the laser light in this fairly thick foil.)

In order to record the position of the foil, a second exposure at reduced streak speed was performed, using a high pressure mercury lamp together with a condensing lens Ko. This brings out in the picture both the contours of the cooling finger, in the centre of which the foil is located, and the edges of the viewing field.

A streak picture obtained in this way is reproduced in Fig. 11. At the time $t = 0$, which coiincides with the beginning of strong absorption in the foil, the matter starts to emit light. On the front side of the foil a bright region extends into the vacuum. This is apparently light emission from the hot plasma produced by absorption of the laser light. From the streak pictures it can be estimated that this plasma expands towards the laser with a velocity of over 10^7 cm/sec. The bright region attains its greatest extent at about the time of the maximum of the laser pulse (when the rate of plasma production is highest) and then declines. The emission observed on the back of the foil is particularly interesting. For a lengthy period no motion of the matter is observed on the back of the foil. The thicker the foil, the longer is this period. If the foil is so thick that it does not become transparent during the laser pulse ($d \geqq 1$ mm), the back remains intact during irradiation.

If the foil becomes transparent during irradiation, as in Fig. 11, the matter is observed to move to the rear a few nanoseconds before the foil becomes transparent. Once the foil has become transparent the movement of the matter apparently stops. Exposing the picture more strongly shows that at this time a plasma jet may possibly be emitted to the rear. It is concluded from the intensity of the emission that this jet is much less intense than that in the forward direction.

Besides the quite distinct burn-through behaviour, which is basic to the understanding of the process of plasma formation (see discussion Sect. IV), the observations with the streak camera provide evidence of the anisotropy of plasma expansion. This applies not only to thick foils ($d \geqq 1$ mm), but also to thin foils ($d < 1$ mm) which become transparent during the pulse. This observation will be confirmed by the interferometric and probe measurements.

In addition, the same camera was used to take single pictures of the phenomenon with an exposure time of 10 nsec [10]. These pictures, not reproduced here, also show that more plasma always expands into the front half-space.

3. *Holographic Interferometry*

It is expected that a fully ionized hydrogen plasma will be produced on the surface of the foil. The refractive index of such a plasma depends in a simple manner on its density. It therefore seems promising to investigate this plasma interferometrically. We use a holographic method which, with a pulse laser as light source, was first described in [12].

The beam path is drawn in Fig. 12. A scatter plate S acts as beam splitter for the laser beam, which is spread by the lens L1. As is necessary for taking a hologram, this plate splits the laser beam into a reference and an object beam. The reference beam is formed by the light transmitted through the scatter plate without deflection (continuous lines). This is focused in the plane of the object (plasma) by the lens L2. The object beam is formed by those beams scattered in S that pass

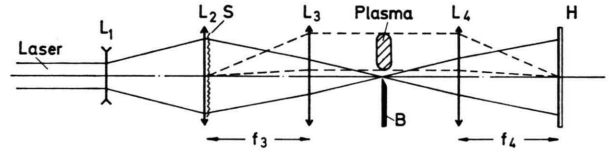

Fig. 12. Optical arrangement for holographic interferometry with scatter plate as beam splitter.

[12] J. M. BURCH, I. W. GATES, R. G. N. HALL, and L. H. TANNER, Nature London **212**, 1347 [1966].

through the lens L3 and reach the field of view. After passing through the lens L4 the reference and object beams produce a hologram on the photographic plate H. The scatter plate consists of a glass flat dusted with magnesium oxide picked up from a magnesium flare. The density of this covering was such that the intensity ratio of the object and reference beam as measured in the plane of the photographic plate was of the order of one.

In order to reconstruct the object, the hologram is irradiated by a point light source (gas laser). Two pictures of the object appear, symmetric to the light source. Overlapping of those two pictures is prevented by darkening the bottom half of the field of view with a mask B during the exposure.

If the hologram is double-exposed, once with and once without plasma, reconstruction yields an interferogram of the plasma. Equidistant interference fringes are obtained if the hologram plate is laterally shifted between exposures. The fringe distance depends on the size of this shift.

Besides the familiar advantages of holographic interferometry (optical components need not be of high precision, coarse adjustment sufficient, no glare from light emission by the object), the arrangement described images the beam splitter, viz. the scatter plate, on the photographic plate. As this reunites every beam split at S, the time and spatial coherence of the light source do not have to be very high. Part of the pulse laser beam can therefore be used for illumination without any filtering.

The set-up for recording the holograms is shown in Fig. 13. A quartz plate (beam splitter) coated on one side reflects 4% of the light emitted by the ruby laser onto a prism. This is the first of a series of prisms that allow the laser pulse to be delayed between the beam splitter and interferometer by utilizing the finite transit time of the light. The delay interval was varied between 1.8 m and 24 m, this corresponding to a delay time of $6-80$ nsec. The prisms were set up with the aid of the adjustment laser. The focal length of the condenser lenses L2 to L4 was $f=15$ cm, that of the divergent lens L1 was $f=-6$ cm. The field of view was bounded

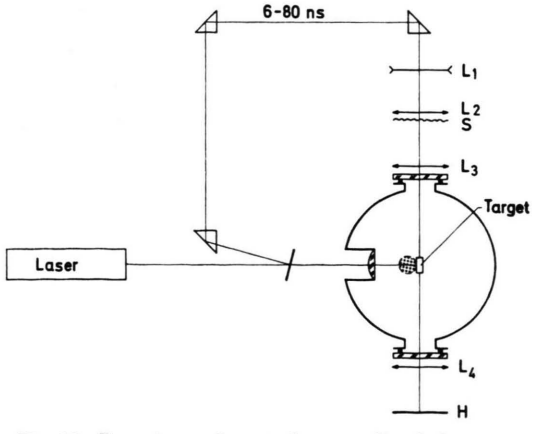

Fig. 13. Experimental set-up for recording holograms.

(diameter 40 mm) by the mounts of the lenses L3 and L4. The focal spot of the reference beam was below the cooling finger. The diaphragm B drawn in Fig. 12 was aligned beneath the cooling finger by means of a rotating lead-through after the bell glass was removed. The hologram plates were of the type Agfa-Gevaert Scientia 10 E 75.

Figure 14 shows two interferograms, each reconstructed from a double-exposed hologram. The cooling finger is seen from the side. The wire attached to the top of the finger points towards the focusing lens. The hole, with the slit pointing to the observer, and the foil itself are not seen since they are obscured by the back part of the finger. The focal spot of the laser, however, is indicated by the bulging of the interference fringes at this point. The black patch at the bottom edge of the pictures covers the focal spot of the gas laser used for reconstruction. It corresponds to the location of the reference beam during exposure of the hologram. As is required, the reference beam does not cross the plasma cloud.

In front of the target the plasma causes a fringe shift on both pictures in Fig. 14. As can be derived from the direction of the plate movement between the two exposures of the hologram, the observed fringe shift corresponds to a medium with refraction index $\eta<1$. With increasing distance from the target the fringe shift becomes smaller, in keeping with the decrease in the optical path length through the plasma due to three-dimensional expansion. At the back of the target the behaviour is different. The top picture is typical of a thick foil ($d \geqq 1$ mm), where no laser light is transmitted before the end of the pulse. With these foils no plasma is observed on the back of the foil. The bottom picture is typical of a thin foil ($d<1$ mm), which transmits laser light. With these foils plasma is observed on the back. However, the amount of plasma is always found to be much smaller on the back than in front of the foil, irrespective of the foil thickness. So these observations again show the anisotropy of the plasma expansion.

The interferograms made with thick foils ($1<d<1.5$ mm) were evaluated quantitatively i. e. the total number N_e of free electrons present in the plasma cloud in front of the target was determined from them.

On the assumption that $\omega \gg \omega_p$ and $\nu/\omega \ll 1$ (ω = laser frequency, ω_p = plasma frequency, ν = collision frequency) the square of the refractive index η of a fully ionized hydrogen plasma is

$$\eta^2 = 1 - \omega_p^2/\omega^2.$$

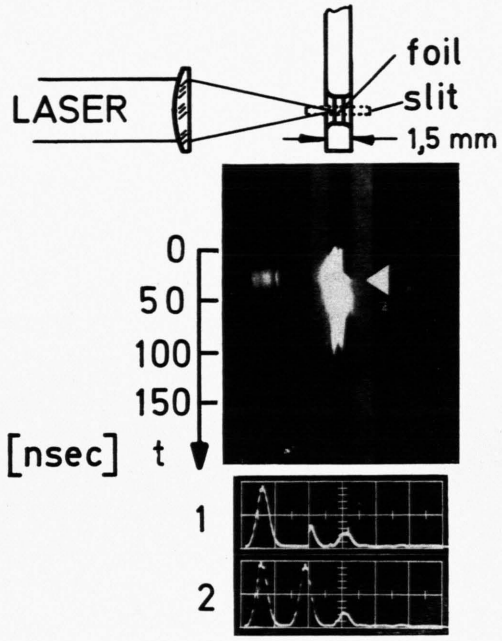

Fig. 11. Streak picture of a laser irradiated hydrogen foil (880 μ thick). Above: cooling finger with slit through which the foil is observed (schematic); streak slit dashed. Centre: streak picture with laser light time marks on both sides. ◀ indicates the time at which strong absorption in the foil ceases. Bottom: oscillogram with the signals D1 to D3. 50 nsec /div. 1) same shot; 2) for comparison with no foil present.

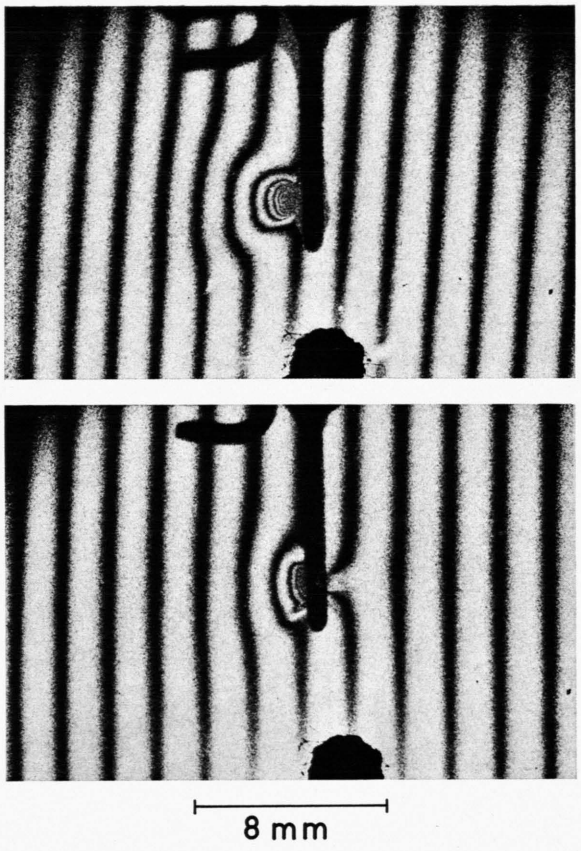

Fig. 14. Interferograms, each reconstructed from a double-exposed hologram. Top: thick foil (1.5 mm). Bottom: thin foil (0.15 mm). Optical delay 18 nsec.

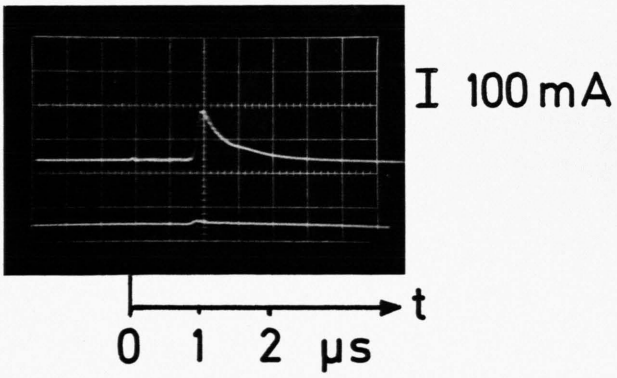

Fig. 16. Signals of the two probes (same sensitivity). Upper trace: probe in front of the target. Lower trace: probe behind the target.

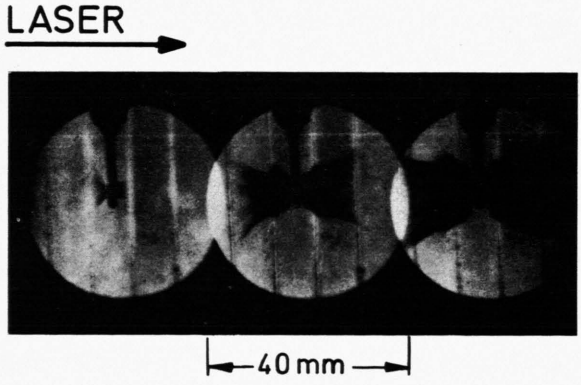

Fig. 17. Expansion of the solid hydrogen disc in the μsec range (three frames at 0.4, 2.4 and 4.4 μsec after laser pulse, exposure time 0.2 μsec each frame). The gas cloud, expanding from the location of the disc at the bottom of the cooling finger, takes the form of two symmetric, black "paint-brushes" which blacken out the background illumination.

After rearrangement and expansion of the root this yields

$$1-\eta=1-\sqrt{1-\frac{\omega_p^2}{\omega^2}}\approx\frac{1}{2}\cdot\frac{\omega_p^2}{\omega^2}=\frac{e^2\,n}{2\,\varepsilon_0\,m_e\,\omega^2}$$

(n = electron density, e = elementary charge, ε_0 = dielectric constant of the vacuum, m_e = mass of the electron).

The two assumptions $\omega \gg \omega_p$ and $\nu/\omega \ll 1$ are satisfied except in the unobserved boundary layer between the plasma and solid, as calculations by MULSER [7] have shown.

As is known, the fringe shift $\varepsilon(x, y)$ caused by a medium of thickness Δ in the point (x, y) of the observed interference field (measured in fringe distances) is

$$\varepsilon(x,y)=\frac{1}{\lambda_0}\int_{\Delta}[1-\eta(x,y,z)]\,dz$$

$$=\frac{e^2\,\lambda_0}{8\,\pi^2\,c\,m_e\,\varepsilon_0}\int_{\Delta} n(x,y,z)\,dz$$

(λ_0 = vacuum wavelength of laser light, c = velocity of light).

The integral should be taken along the beam (z-direction) which passes through the interference field at the point (x, y). The total number N_e of free electrons in the plasma is found by integrating over the area covered by the plasma

$$N_e=\int_F\left[\int_{\Delta} n\,dz\right]dF=\frac{8\,\pi^2\,c^2\,m_e\,\varepsilon_0}{e^2\,\lambda_0}\int_F \varepsilon(x,y)\,dF\,.$$

In order to obtain N_e, the interference field is divided into small elements of area dF_ν and the fringe shift ε_ν is determined in each element. The above integral, and hence N_e, is then obtained by forming the product $\varepsilon_\nu \cdot dF_\nu$ and by summation.

Particular attention was thereby paid to two sources of error:

a) As a result of expansion the plasma cloud is highly rarefied at the boundary, and so it does not cause any measurable fringe shift. As the front velocity of the plasma is known from probe measurements, the area covered by the plasma when the picture is taken can be bounded towards the vacuum. At the plasma boundary thus defined the fringe shift should be set equal to zero. The fringe shift in the boundary region of the plasma can then be determined as well by interpolating between the region of distinct fringe shift and the boundary.

b) In the immediate vicinity of the target the interference fringes are no longer resolved. This region has therefore to be excluded from evaluation, although the electron density is particularly high there during irradiation. The error that would thereby result is avoided by evaluating pictures taken with increasing optical delay time τ_b. As no more plasma is produced on termination of the laser pulse but the plasma continues to expand, the number of electrons in the region near the target that is not evaluated becomes negligible some time after the end of the laser pulse. It is therefore expected that with increasing delay time the total number of free electrons observed approaches the actual value present.

The result of the evaluation is presented in Table 1. For each delay time about ten shots were evaluated. From the increase of N_e with delay time τ_b it is evident that N_e has virtually attained its final value after 31 nsec. Interferograms with a longer delay time were not evaluated since the edge of the plasma is no longer in the field of view and also the fringe shift disappears with time as a consequence of the expansion.

So in the case of thick foils ($1 < d < 1.5$ mm). which absorb the entire laser pulse, the total number of free electrons in the plasma as determined by interferometry is 4.1×10^{16} electrons.

τ_b	6 nsec	18 nsec	31 nsec
N_e	2.2×10^{16}	3.6×10^{16}	$(4.1\pm0.3)\times10^{16}$

Table 1. Total number N_e of free electrons in the plasma as a function of the optical delay time.

4. Charge Collection and Time-of-Flight Measurements

Using a suitable charge separation probe to measure the ion current flowing from the target into a certain solid angle, it is possible by integrating over the half-space to find the total number of ions in the plasma. From the time of flight between the target and probe it is also possible to determine the kinetic energy of the ions.

Even without detailed knowledge of the plasma production process it is possible to form some idea of the expansion of the plasma. We consider a plasma cloud with the initial radius R_0 and the internal energy U_0 generated by irradiating the foil. This plasma cloud expands adiabatically into the vacuum since there is no further energy input after the short heating phase. As a result of the expansion the internal energy of the plasma is completely converted with time into directed kinetic energy. From the equation of state $p\,V = (\gamma - 1)\,U$ and the adiabatic law $p\,V^\gamma = \text{const}$ it follows that the decrease of the internal energy with the radius is $U \sim R^{-3(\gamma-1)}$. With $\gamma = 5/3$ (fully ionized plasma) one obtains $U \sim R^{-2}$.

As long as the internal energy is still comparable with the kinetic energy of the plasma, the individual volume elements generally follow curved paths under the influence of the pressure prevailing in the plasma. Finally, when the internal energy can be neglected relative to the kinetic energy of the plasma, there are no longer any forces acting on the individual volume elements; by virtue of their inertia they move radially outwards in a straight line with constant velocity. If the diameter of the focal spot ($\approx$0.1 mm) is taken as initial radius R_0, it is found as a result of the quadratic decrease of the internal energy with the radius that for $R = 1$ mm 99% of the internal energy has already been converted into kinetic energy of the plasma. Thus, for an observer at a comparably large distance from the target the volume elements of the plasma describe straight paths originating where the plasma is produced. For this observer the density of the plasma stream decreases proportionally to $1/r^2$ (r = distance target – observer).

With equal ion and electron temperatures in the plasma the electrons have a higher thermal velocity than the ions owing to their small mass. In the course of expansion the undirected thermal motion of the two types of particles changes to directed motion. Both the ion and the electron temperature thereby go to zero. As it is expected that the plasma remains electrically neutral on expanding, the velocity of the electrons should become equal to that of the ions during expansion. In view of the large difference in mass between ions and electrons this means that the energy of the plasma at a large distance from the target is in the form of kinetic energy of the ions. Therefore if the velocity, and hence the kinetic energy, of the ions is determined by a time-of-flight measurement, this yields on multiplying by the number of ions the energy absorbed by the plasma (without dissociation and ionization energy).

The measurements were made with two identical probes that are shown in Fig. 15. They consist of a long metal tube that can be shifted longitudinally. The axis of the tube points to the target. The plasma enters the probe through an opening 2.5 mm in diameter that is covered by a perforated grid. These perforations are 0.12 mm in diameter, and the geometrical permeability of the grid is 33%. The tube and grid are both at ground potential. At a distance of about 1/2 mm from the grid is a collector at negative potential (-120 V).

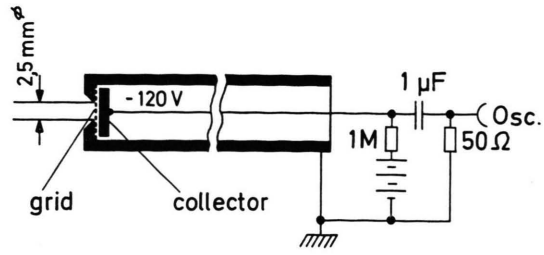

Fig. 15. Probe with circuitry.

It is to be expected that the electrically neutral plasma streaming in through the grid will be separated into ions and electrons in the electric field of the probe. While the ions are accelerated towards the collector by the field, the electrons are kept away from it. The ions deposit their charge at the collector. The ion current entering the probe through the grid can therefore be measured time resolved as collector current.

In order to check whether the behaviour of the probes comes up to expectations, it was investigated experimentally prior to the actual measurements by varying the collector potential and the target-to-probe distance. For these investigations a mylar target was used.

1. A few volts of negative potential at the collector are already sufficient to saturate the probe signals; i. e. any further increase of the negative potential at the collector does not affect the signals. It is concluded from this that:

a) the ions and electrons are completely separated;

b) the kinetic energy of the electrons is less than a few eV.

2. If the sign of the potential at the collector is changed (positive), the signal also changes sign. A voltage of several hundred volts is required, however, to saturate the signals, i. e. first this potential value has to be attained before the ions stop reaching the collector. As we shall see, a value of this order of magnitude is obtained for the kinetc energy of the ions from their time of flight.

3. The ion velocity calculated from the time of flight does not depend on the target-to-probe distance, which was varied between 10 – 70 cm. The path along which the ions are acelerated during expansion is thus very small and can be neglected in calculating the velocity from the time of flight and path length (20 cm in the measurements).

4. The ion current decreases with increasing target-to-probe distance in proportion to $1/r^2$.

So these measurements confirm our conception that the plasma undergoes a three-dimensional expansion as a result of its inertia.

The two identical probes were mounted at a distance $r = 20$ cm from the target. They were placed in front of and behind the target, each at an angle of 45° to the laser axis. Figure 16 shows typical signals. The time of the laser pulse ($t = 0$ in this time scale) is marked by a signal of photoelectrons that are liberated in the probe as a result of the light emission from the initially hot plasma. After about 1 μsec the fastest ions (with a kinetic energy of 400 eV) reach the probe. The current steeply rises to a maximum and then tends back to zero. The different signal levels of the two probes again show that the greater part of the plasma expands into the front half-space, this being in agreement with the observations made with the other techniques.

The number N_K of ions impinging on the collector is obtained by integrating the current i over the time:

$$N_K = \int_0^\infty i(t)\, dt/e$$

(e = elementary charge).

The mean kinetic energy of the ions striking the collector is found by averaging over the ion velocity calculated from the time of flight:

$$\overline{E}_{45^0} = \frac{m_p}{2}\overline{v^2} = \frac{m_p r^2}{2}\int_0^\infty \frac{i(t)}{t^2}\, dt \Big/ \int_0^\infty i(t)\, dt$$

(m_p = proton mass).

The total number N_i and the mean kinetic energy $\overline{E}$ of the ions expanding into the front and back half-spaces were determined from the signals of the two probes by integrating over the relevant half-space. The integration was based on the angular distributions measured by OPOWER and PRESS [13] on a LiH target under similar conditions.

The values thus obtained are listed in Table 2. The values with error margins are mean values from a large number of shots (approximately 30). What is given is the mean quadratic error of the result. The values without error margins are intended to show the response of the particular quantity to the foil thickness. These values are based on a smaller number of shots. We mention especially two facts:

1) Again the strong anisotropy of the plasma expansion is observed.

2) The number of ions evaporated from thick foils ($1 < d < 1.5$ mm) agrees well with the number of free electrons in the plasma determined interferometrically.

5. Three-image Photographs in the μsec Range

The image-converter camera, now without the streak slit and the light pipes, was used to take three-image pictures in the μsec range. These pictures are intended for observing not the hot plasma, which at these late times has already reached the walls of the vacuum chamber, but the subsequent behaviour of the hydrogen disc after being hit in the centre by the laser.

The three pictures in Fig. 17 show an expanding gas cloud that darkens the background illumination. The gas cloud emanating to both sides from the hydrogen disc in the cooling finger takes the form of two black "paint-brushes" that are approximately symmetric to the axis of the laser beam. The fronts formed by the tips of these brushes move with a velocity of 5.5×10^5 cm/sec. As subsequent pictures show, the gas cloud finally darkens the entire field of view, which does not become bright again till after about 20 μsec. The disc has meanwhile completely evaporated.

Thus, so much energy is transferred to the whole of the disc from the small irradiated region that it evaporates completely. As will become clear from Section IV, the energy transfer should be due to shock waves emanating from the focus region. These shock waves will distribute their energy content within a time of the order of the laser pulse length more or less uniformly over the whole volume of

d [mm]	0.2	0.5	0.8	1.0	$1 < d < 1.5$
$N_{i,\,front}$	2.6×10^{16}	3.1×10^{16}	3.6×10^{16}	4.0×10^{16}	$(4.3 \pm 0.3) \times 10^{16}$
$N_{i,\,back}$	0.3×10^{16}	0.6×10^{16}	0.3×10^{16}	0	0
$\overline{E}_{front}$ [eV]	120	190	190	190	193 ± 6
$\overline{E}_{back}$ [eV]	120	190	190	/	/

Table 2. Total number N_i and mean kinetic energy $\overline{E}$ of the ions in the plasma as functions of the foil thickness d.

[13] H. OPOWER and W. PRESS, Z. Naturforsch. **21 a**, 344 [1966].

the hydrogen disc. If the front velocity of the observed brushes is interpreted as the front velocity of a rarefaction wave emanating subsequently from the disc, the energy transferred to it can be estimated [10]. It is found under these assumptions that more than 20% of the absorbed energy is transferred to that part of the disc which is not transformed into a hot plasma during laser irradiation.

IV. Discussion of the Experimental Results

1. The Problem of Plasma Production by Laser in One-dimensional Plane Geometry

The problem of producing plasmas by intense laser radiation has been investigated theoretically by several authors [5–7] in one-dimensional plane geometry. As we shall be comparing the experimental observations with these theoretical results, it is worthwhile to summarize briefly the main results of one-dimensional theory.

In all the papers cited the process of plasma formation by strong laser radiation is treated as a gasdynamic process. The flow of matter, which is assumed to be an ideal gas of ions and electrons, is described by the one-dimensional fluid equations. The absorption of the laser light due to inverse bremsstrahlung is taken into account locally. The initial conditions are: At the time $t=0$ the laser is switched on with constant intensity Φ_0. The laser light emerges from the vacuum and irradiates the surface of the solid hydrogen (density ϱ_0), which either fills the half-space [5, 6] $x \leqq 0$ or takes the form of a solid hydrogen foil [7]. The various investigations essentially lead to the same results, the main difference being the method by which solutions of the set of differential equations are found. We briefly outline the work of MULSER [7], where integration of the equations is performed numerically on a computer.

Owing to the high intensity a breakdown in the solid occurs, which, within a fraction of a nanosecond, leads to complete absorption of the laser light in a thin layer at the surface of the solid hydrogen. This early stage of the process, however, is not the process under investigation here.

During the subsequent heating a density profile forms which maintains its characteristic shape during irradiation (Fig. 18). The space can be divided into three regions with different states of matter, viz. a hot plasma (region 2), a shock wave (region 1), the undisturbed solid (region 0). The plasma region is separated from the shock wave region by a narrow zone of strong density variation. A great part of the incident laser light crosses the plasma region and is then absorbed in this layer, which is denoted in the following as the deflagration front F. A shock front S separates the shock wave region from the undisturbed solid. The various regions as well as F and S are denoted in Fig. 18 in the density profile for $t=1.5$ nsec.

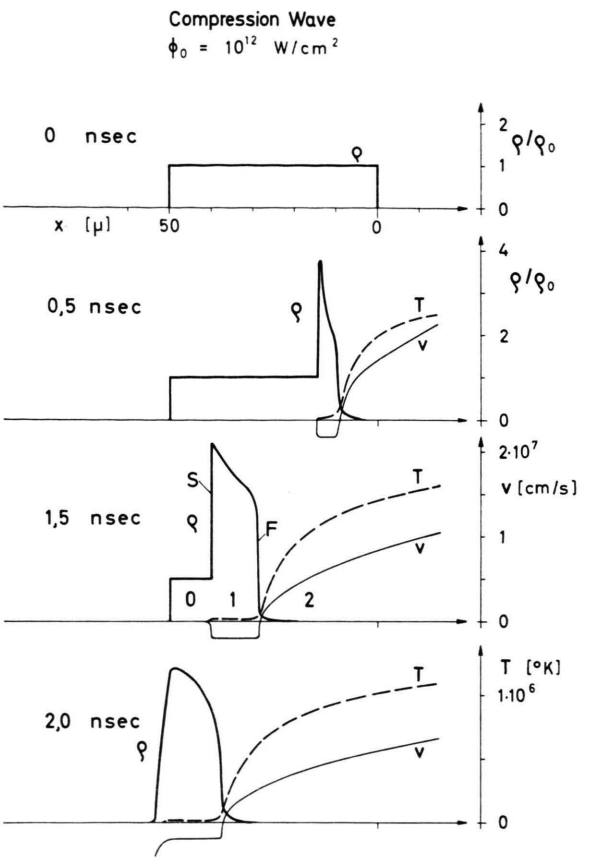

Fig. 18. Shock wave in a laser irradiated solid hydrogen foil [7]. Laser from the right. The numbers in the curve at 1.5 nsec denote regions with different states of matter: 2 hot plasma, 1 shock wave, 0 undisturbed solid. F deflagration front, S shock front.

In the plasma region (2) at an intensity of $\Phi_0 = 10^{12}$ W cm^{-2} a temperature of about 2×10^6 °K is achieved within 18 nsec (halfwidth of our laser pulse). The density of the plasma (at the location of the temperature maximum) is 10^{-2} to 10^{-3} times as small as the density of solid hydrogen. The flow velocity of the plasma is directed towards the laser and is of the order of some 10^7 cm sec^{-1}. Whereas at the beginning nearly all of the laser light reaches F, absorption in the plasma ahead increases with time. This increase in absorption is particularly pronounced in a one-dimensional model since the plasma then always remains in the radiation field of the laser.

The steep density gradient in the deflagration front F, where the plasma is produced, has, of course, to do with the fact that the laser light cannot penetrate more than about a wavelength into a plasma with $\omega_p > \omega_{Laser}$ ($\omega_p = \omega_{Laser}$ is achieved at an electron density $n_e \approx 3 \times 10^{21}$ cm^{-3}, whereas the density of atoms in solid

hydrogen is 4.56×10^{22} cm^{-3}). The problems related to this layer, including that of reflection, are discussed in [7].

Behind the shock front S, i. e. between S and F, dense matter streams away from the laser. On passage through the shock front S the solid hydrogen is compressed by a factor 4. This is due to the fact that S is a strong shock and the solid hydrogen is assumed to be an ideal gas with $\gamma = c_p/c_v = 5/3$. The velocity of S is $v_s = 2.7 \times 10^6$ cm sec^{-1} and is practically constant in time. The temperature in the shock wave is about 1.5×10^4 °K, the pressure about 300 Kbar. Only about 10% of the incident energy is transferred to the shock wave, whereas 90% is converted to thermal and kinetic energy of the hot plasma. Since no laser light penetrates into the shock wave region, the energy contained in the shock wave is, of course, compression work performed on the solid by the pressure of the hot plasma.

At the moment where the shock front reaches the back surface (after about 2 nsec for the 50 μ-foil of Fig. 18) a rare faction wave develops. During the subsequent phase the dense compressed part of the foil is accelerated as a whole by the pressure of the plasma. This, however, is of little influence on the process of plasma formation and heating which is still taking place in F.

The mass of the hot plasma produced is shown in Fig. 19 as a function of time for the case where the solid hydrogen fills the half-space $x \leqq 0$. It is given as the layer thickness of the evaporated material (related to the density of solid hydrogen ϱ_0).

2. *Comparison of the Experimental Results with Theory*

A quantitative comparison between the measured values and those calculated for the one-dimensional plane geometry in [7] is afforded by Table 3. The experimental values apply to foils between 1 mm and 1.5 mm thick that do not become transparent during irradiation.

	Theory [7, 14]	Experiment	
N	1.5×10^{16}	$N_e = 4.1 \times 10^{16}$ $N_i = 4.3 \times 10^{16}$	Laser data:
$\overline{E}$	1×10^3 eV	200 eV	$\Phi = 10^{12}$ W/cm^2,
E_2/E_L	0.9	0.45	$E_L = 2.9$ joule,
E_1/E_L	0.1	>0.2	$\tau = 18$ nsec,
v_s	2.7×10^6 cm sec^{-1}	3×10^6 cm sec^{-1}	$2r_0 = 0.14$ mm.

Table 3. Comparison of calculated and measured values.

The experimental values given are the total number of ions N_i and electrons N_e in the plasma. These were determined by independent methods, viz. charge collection measurement and interferometry respectively, and agree within the margins of error. For the energy E absorbed by each evaporated atom we give the mean kinetic energy of the ions that is determined from the time-of-flight measurements. The product of the total number and the kinetic energy of the ions yields the energy E_2 of the plasma (without dissociation and ionization energies). It is given as the ratio E_2/E_L between the value thus calculated and the absorbed laser energy E_L. In addition, we also give the ratio of the energy E_1/E_L transferred to the dense matter (estimated in Section III.5) to the absorbed energy E_L and also the measured velocity of the shock wave v_s.

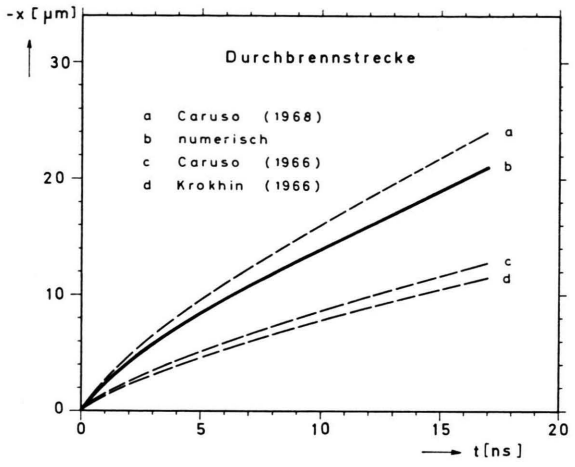

Fig. 19. Mass of evaporated plasma expressed in layer thicknesses of the solid [14].

The theoretical values are taken from MULSER [7, 14]. The number N of evaporated atoms is obtained from Fig. 19 (for the given laser data). Since 90% of the energy input is transferred to the plasma and 10% to the shock wave, we get $E_2/E_L = 0.9$ and $E_1/E_L = 0.1$. $\overline{E}$ is obtained from the relation $\overline{E} = 0.9\, E_L/N$ from which value the ionization and dissociation energies have, strictly speaking, still to be deduced.

Comparison between the measured and calculated values in Table 3 shows that agreement is found only with respect to the order of magnitude. This is not surprising since comparison is done with values calculated in one-dimensional geometry. Such calculations can strictly be valid only in the case of a laser beam of infinite lateral extent, whereas in the experiment the focused beam covers only a small area. One can, however, argue that the deviations occur in the right direction:

1) As Table 3 shows, more plasma, but with less energy, is produced. There are two reasons, in particular, for this:

a) As a result of the three-dimensional expansion the absorption in the plasma is less pronounced than

[14] P. MULSER and S. WITKOWSKI, Phys. Lett. **28 A**, 151 [1968].

in the one-dimensional case. Therefore more light reaches the deflagration front and more plasma is produced. As the absorbed energy is thus distributed over more atoms, the mean energy per atom is lower.

b) Focusing causes the diameter of the focal spot to change along the path of the deflagration front. On the average (particularly for thick foils) it is larger than at the point where the beam cross section is narrowest. Furthermore, the focal spot of the laser was possibly enlarged by the spherical aberration of the uncorrected lens. Enlarging the focal spot at a fixed energy E_L and half-width τ of the laser pulse also results in increased plasma production [6]:

$$\frac{d\mu}{dt} \sim \pi r_0^2 \Phi^{1/2} = \pi r_0^2 \left(\frac{E_L}{\pi r_0^2 \tau}\right)^{1/2} \sim r_0 .$$

2) As can be seen from Table 3, the percentage of energy transferred to the dense matter (more than 20%) is higher than that calculated for the one-dimensional case (10%). The reason for this high value may be that, unlike in the one-dimensional case, the plasma performs compression work on the solid not only in the deflagration front F, but also along the channel created by the laser. The formation of this chanel wil be discussed below.

The measurements were checked by an energy balance. 45% of the energy input reappears as kinetic energy of the plasma (see Table 3). If allowance is made for the dissociation and ionization energies that have to be made available for producing the plasma (15.8 eV per atom altogether), this value is raised by 8%. More than 20% of the energy input is transferred to the dense matter (see Table 3). Altogether this accounts for more than 70% of the energy input.

The energy balance shows that we can discount the possibility that a large part of the energy input has escaped observation as kinetic energy of neutral atoms that recombine during the expansion of the plasma. The presence of strong recombination in the plasma is also refuted by the fact that the number of electrons and protons observed in the plasma is consistent at widely spaced times (30 nsec and 1 μsec after the laser pulse).

3. Burn-through Behaviour of the Foils

Whereas reasonable agreement was found between the calculated and measured properties of the plasma, the observed burn-through behaviour of the foils can only be explained by extending the one-dimensional theory. This is illustrated by the following:

1) The absorption measurements revealed the existence of a time interval of strong absorption, i. e. the burn-through time t_D. This was measured to be 34 nsec for a foil of 1 mm thickness (Fig. 7). According to the one-dimensional theory this time interval should be determined by the time at which the foil is completely transformed into a hot plasma. The rate of plasma production is given by the slope of the curves in Fig. 19. After 10 nsec the slope of curve b corresponds to a velocity of about 1×10^5 cm sec^{-1}. This value, which depends only weakly on time and foil thickness [7], gives for a foil of 1 mm thickness a burn-through time of the order of 1 μsec. This is about 30 times the measured value.

2) As the interferometric and charge collection measurements have shown, about 4×10^{16} atoms are vaporized as a hot plasam from a foil of 1 mm thickness. The focus region, however, contains at least 7×10^{17} atoms, assuming a cylinder with diameter $2 r_0 = 0.14$ mm and height $h = 1$ mm. As such a foil becomes transparent to the laser light at the end of the pulse, the question arises what happens to the rest of the atoms, i. e. the much greater part.

As will become clear below, explanation of these effects needs, in principle, a two-dimensional treatment of the light-solid interaction. As a rigorous treatment of this problem seems rather difficult, we restrict ourselves to a rough, qualitative description which treats the problem by analogy with a piston moving with hypersonic velocity. The following remarks relating to foils follow the same lines as those in [6] for the case of small pellets.

The introduction of the piston concept results from an analysis of the ϱ-curves in Fig. 18. The analysis shows that the matter picked up by the shock front collects between S and F, as if the deflagration front F were acting as a piston impermeable to matter. [This also results from a comparison between the velocity of the shockwave (2.7×10^6 cm sec^{-1}) and the velocity corresponding to the rate of plasma production (1×10^5 cm sec^{-1}, see above).] Of course, the hypothetical piston F is acted on by the pressure of the plasma produced in F.

The interaction of the focused beam with the solid is expected to proceed as follows: At the beginning the laser pulse breakdown in the foil oc-

curs and the deflagration front F forms on the surface of the solid. Subsequently a shock front S gradually moves away from the deflagration front F, and between S and F a pressure of the order of 10^5 atm is produced. Whereas during this early stage the interaction is one-dimensional and the shock front is plane, one would expect that with increasing distance between S and F owing to the finite diameter of the focused beam the shock front tends to become curved. The situation is sketched in Fig. 20, where for simplicity the focused beam is replaced by a collimated beam with the diameter $2\,r_0$, equal to the diameter of the focal spot. We now consider the deflagration front F as the front face of a piston which, of course, is not of infinite lateral extent, but has the diameter of the focused

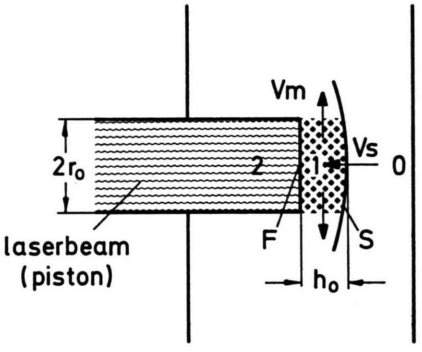

Fig. 20. Piston model used to describe the interaction of a focused laser beam with a solid hydrogen foil.

beam. This piston, moving with hypersonic velocity, causes a curved shock wave, i. e. a bow shock. This means that the matter picked up by the bow shock is due to the high pressure behind the shock front streaming out of the dotted cylinder (Fig. 20) in radial direction (for a co-moving observer) since it cannot penetrate the impermeable front face of the piston. If we assume a constant velocity of the piston, the bow shock will become stationary after covering a distance of the order of the piston diameter. This means that the distance between the shock front and the deflagration front no longer increases, but they move together at the same velocity. As in the one-dimensional model, a distinction is again made between the three regions (see Fig. 20): undisturbed solid (0), shock wave (1), and hot plasma (2).

The characteristic flow of matter behind the bow shock has the essential consequence that during the passage of the shock front and the deflagration front through the foil a large amount of the matter originally located in front of the laser beam may leave the focal region without being transformed into a hot plasma. Thus one of the discrepancies between experiment and one-dimensional theory mentioned at the beginning of this section has been cleared up. It should be mentioned, however, that this flow of matter is made possible by the high compressibility of solid hydrogen and is probably less pronounced in other materials which are less compressible.

In order to estimate the distance between the shock front and deflagration front, we have to imagine an observer moving with the shock front. For this observer matter of density ϱ_0 streams with the velocity v_s through the shock front into the dotted cylinder in Fig. 20. Matter of density ϱ_1 escapes with the velocity v_m at the sides through the cylinder jacket. Since the mass inflow must be equal to the mass outflow under stationary conditions, it holds that

$$\pi\, r_0^2\, \varrho_0\, v_s = 2\,\pi\, r_0\, h_0\, \varrho_1\, v_m\,.$$

If it is assumed that

$$v_m = v_s/2\,,$$

one obtains

$$h_0 = r_0\, \varrho_0/\varrho_1\,.$$

With $\varrho_1/\varrho_0 = 4$ one obtains $h_0 = r_0/4$, i. e. a shock front-to-deflagration front distance of $18\,\mu$ for a focal spot diameter of 0.14 mm. The value $v_m = v_s/2$ was chosen because this gives the correct shock wave-to-surface distance for a sphere moving with hypersonic velocity in the limiting case of high Mach number [15]. (A curved deflagration front will, in fact, be present in the experiment because the intensity distribution over the focal spot decreases towards the periphery.)

Assuming a constant velocity the shock front reaches the back surface of the foil after the time $t_s = d/v_s$. We may describe the further course of events as follows (Fig. 21): The matter contained in the dotted cylinder between S and F is accelerated to the rear by the continued reaction of the plasma still being produced in F. The height of the cylinder thereby continues to decrease because matter keeps flowing out in the radial direction whereas matter no longer enters the cylinder through its front face. As with decreasing height of the cylinder the mass outflow in the radial direction goes to zero, the small, but finite, mass loss due to vaporization in F then becomes important for the "lifetime" of the dense phase in front of the laser beam. Finally, there is no longer any dense matter in the laser beam, and the deflagration front F disappears. This

[15] H. OERTEL, Stoßrohre, Springer-Verlag, Vienna — New York 1965, S. 819.

break-up of the foil terminates the period of strong absorption, and the laser beam can pierce the foil through the channel it has created.

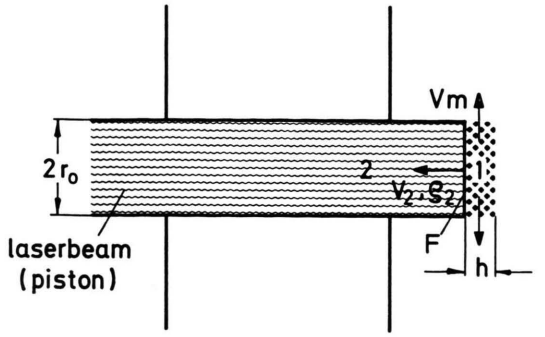

Fig. 21. Piston model after penetration to the back of the foil.

The time t_b that elapses between the arrival of the shock wave at the back of the foil and the disappearance of the deflagration front can be estimated. The differential equation for the decrease of the height of the cylinder due to the escape and vaporization of matter is (Fig. 21):

$$\pi r_0^2 \varrho_1 \frac{dh}{dt} = -2\pi r_0 \varrho_1 v_m h - \pi r_0^2 \varrho_2 v_2$$

where ϱ_2 and v_2 denote the density and velocity of the plasma produced in F. All quantities apart from h are assumed to be independent of time. (It holds that $v_2 \varrho_2 \sim t^{-1/4}$, see [6].) From the solution of the differential equation we obtain with the conditions $h = h_0 = r_0 \varrho_0/\varrho_1$ for $t = 0$ and $h = 0$ for $t = t_b$ the following expression for t_b:

$$t_b = \frac{r_0}{2 v_m} \ln\left(\frac{2 \varrho_0 v_m}{\varrho_2 v_2} + 1\right).$$

We again set $v_m = v_s/2$ ($v_s = 2.7 \times 10^6$ cm sec^{-1}). The product $\varrho_2 v_2$ can be calculated if it is borne in mind that $\pi r_0^2 \varrho_2 v_2 \tau = \mu$ where μ is the mass evaporated by the laser under one-dimensional conditions. This can be found from Fig. 18 as the layer thickness δ ($\delta \approx 20 \times 10^{-4}$ cm for $\tau = 18$ nsec) of the evaporated solid (density ϱ_0). Because $\mu = \pi r_0^2 \varrho_0 \delta$ the above equation becomes

$$t_b = \frac{r_0}{v_s} \ln\left(\frac{v_s \tau}{\delta} + 1\right).$$

With the given numerical values we then get

$$t_b = 3.2\, r_0/v_s\,.$$

On comparing t_b with t_s it is found that the burn-through time $t_D = t_s + t_b$ for thick foils ($d \gg 3.2\, r_0$) is governed essentially by the time of passage t_s of the shock wave. Thus, dividing the thickness d of a foil by the burn-through time t_D measured should yield the velocity of the shock front. With $d = 1$ mm and $t_D = 34$ nsec (from Fig. 7) one gets $v_s = 3 \times 10^6$ cm sec^{-1}, which agrees surprisingly well with the calculated value [7] $v_s = 2.7 \times 10^6$ cm sec^{-1}.

If we now examine the experimental observations in detail, we find some more evidence of the applicability of the model:

The absorption measurements show that strong absorption in the foil occurs at the beginning of the pulse. This indicates that the deflagration front F has formed. The deflagration front and shock front, which subsequently should pass through the foil a small distance apart and with the same velocity in accordance with the model, could not be observed direct because the lens effect of the convex disc surface facing the observer prevents observation of the processes inside the disc. The persistently strong absorpton in the foil (see absorption measurements) and the escape of plasma towards the laser (as seen in the streak photographs) are, however, indirect confirmation of the existence of the deflagration front F. The absence of substantial reflexion during this time interval also agrees with theoretical predictions [7].

During the time t_s taken by the shock front to pass from one side of the foil to the other, the back surface of the foil should remain undisturbed. As the streak picture clearly shows, such an interval is in fact observed. In Fig. 11 this time is about 25 nsec. During this period no motion of the matter is observed, thus showing that the matter on the back of the foil remains in the cold state. At a certain time matter is suddenly observed to move to the back. At this time the shock front reaches the back surface of the foil. The matter is heated by this shock wave and set in motion. The foil, however, is not yet permeable to the laser light. A thin layer of dense matter will still be located in the laser beam. According to our estimate the time t_b that elapses until the foil becomes transparent should be small relative to the time of passage t_s of the shock front. The intensity of the transmitted laser light does in fact rise steeply a few nanosecond later, thereby indicating the disappearance of the deflagration front.

A final consequence of this piston model is that the bulk of the plasma should always expand into the front half-space. This was clearly observed with various diagnostic methods (streak photography, interferometry, charge-collection measurements). A comparatively small amount of plasma expanding into the back half-space was observed in accordance

with the model only with thin foils which are pierced by the laser light. It should be noted that momentum is conserved in our model since the recoil momentum of the plasma expanding into the front space is transferred to the dense matter of the foil.

Our discussion was based mainly on the results from thick foils ($d \geqq 1$ mm). This is appropriate to the rough model applied, which takes into account neither the variation in space of the light intensity in the vicinity of the focal spot nor its time variation. Thus, for example, the velocity of the shock wave as determined experimentally from the absorption measurements is only the mean velocity in a thick foil. We do not aspire to explain in detail the dependence of the burn-through time (Fig. 7) or of the number of particles in the plasma (Table 2) on the foil thickness. In order to do this in a meaningful way, a model more adapted to the experimental conditions should be used, and, in addition, more detailed measurements, possibly including the break-down process, should be made. The expansion and absorption behaviour as observed with streak camera and photodiodes remains quite pronounced, however, down to foils with a thickness of about 0.2 mm, thus indicating that essentially the same shock wave mechanism takes place. Up to now the experimental investigation has not been extended to thinner foils.

Among the numerous observations made by other authors we restrict ourselves to mentioning those closely related to our experiment. The dependence of burn-through time on foil thickness measured in [16] on thin mylar foils was explained in [17] in a similar manner to here. The existence of, at the same time, the hot plasma and a dense phase, which leaves the focal region partly unburned, was detected in [4] with solid deuterium pellets. This observation was also explained on the basis of one-dimensional theory [16]. Unidirectional plasma expansion from small spheres of paraffin was also found in [18].

The experiment which is closest to ours is described in [19], where a solid deuterium block is used as target. Streak photographs show also the characteristic expansion behaviour of the plasma observed here. Through the clear side surface the propagation of a luminous front in the interior of the block could be observed. With this front, whose velocity is of the order of 10^6 cm/sec, it could not be discriminated whether it would be the shock-front or the deflagration front. This might in fact be difficult since they will follow each other, according to our considerations, at a small distance only. In this experiment, where a more intense laser is used, emission of neutrons could recently be observed [20].

Acknowledgements

The author is indebted to Prof. R. WIENECKE for his encouragement and continued interest in this work. He also wishes to thank Dr. S. WITKOWSKI for many helpful discussions in the course of this work. The technical assistance of H. KOLENDA, H. KRAUSE, and P. SACHSENMAIER is gratefully acknowledged. — This work was performed as part of the joint research programme of the Institut für Plasmaphysik and EURATOM.

[16] W. G. GRIFFIN and J. SCHLÜTER, Phys. Lett. **26 A**, 241 [1968].
[17] A. CARUSO and R. GRATTON, Phys. Lett. **27 A**, 48 [1968].
[18] E. FABRE and H. LAMAIN, Phys. Lett. **29 A**, 497 [1969].
[19] J. L. BOBIN, F. DELOBEAU, G. DE GIOVANNI, C. FAUQUIGNON, and F. FLOUX, Nuclear Fusion **9**, 115 [1969].
[20] F. FLOUX, D. COGNARD, J.-L. BOBIN, F. DELOBEAU, and C. FAUQUIGNON, C. R. Acad. Sci. Paris **269 B**, 697 [1969].